The Reverse Anomeric Effect in *N*-Pyranosylimidazolides: A Molecular Orbital Study

Stewart S. C. Chan, Walter A. Szarek, Gregory R. J. Thatcher*
Department of Chemistry, Queen's University, Kingston, Ontario K7L 3N6, Canada

The reverse anomeric effect was defined by Lemieux to describe the observation of an equatorial preference for quaternary ammonium substituents at the anomeric position of a pyranoid ring. This is contrary to the predictions of the generalized anomeric effect. Subsequent redefinitions have extended the effect, but recently the very existence of the reverse anomeric effect has been questioned. Whereas previous computational studies have focussed on $-NHR_2^+$ substituents, this paper uses AM1 and *ab initio* calculations (up to MP2/6-31G*//RHF/6-31G*) on *N*-pyranosylimidazolides and a truncated model system to ascertain the existence, generality and cause of the reverse anomeric effect. Torsional energy profiles, natural bond orbital (NBO) analysis and electrostatic and solvation interactions have been calculated for isomers of three methoxymethylimidazolides [CH_3OCH_2Im: unsubstituted (**3**), 2-fluoro (**4**) and 2-methyl (**5**) imidazoles]. The axial imidazolides are dominated by two large counteracting contributions: stabilizing anomeric hyperconjugation and destabilizing 1,3-diaxial steric effects. Comparable hyperconjugative and steric effects are greatly diminished in the equatorial isomers. The conformational equilibria are thus very sensitive to small stabilizing electrostatic and hydrogen bonding interactions, which are evident in the protonated imidazolides, and especially pronounced in the equatorial conformers. Imidazolides **3** and **4** show a shift in equilibrium on protonation towards the equatorial conformation compatible with the presence of the reverse anomeric effect, but the same shift is not calculated for imidazolide **5**. Furthermore, calculation of solvation energies suggests that any reverse anomeric effect may be diminished or disappear on moving to more polar solvents. The data for imidazolide **3** are compatible with experimental data, but these calculations suggest that the reverse anomeric effect is not a general phenomenon even for quaternary ammonium substituents at an anomeric centre. The causes of the reverse anomeric effects observed in both **3** and **4** are stabilizing electrostatic interactions in the protonated equatorial conformers.

The generalized anomeric effect (GAE) describes the preference for synclinal over antiperiplanar conformations in the 'anomeric fragment' W–X–Y–Z, where X is an atom possessing one or more pairs of non-bonding electrons, Z is electron-withdrawing and W and Y are atoms of intermediate electronegativity (Y is usually carbon).[1] Manifestations of the GAE in carbohydrate chemistry extend from the Edward–Lemieux effect[2] to the exo-anomeric[3] and reverse anomeric effects.[4] These conformational phenomena have primary importance in control of the structure and presumably function of the many important biomolecules containing monosaccharides, oligosaccharides, nucleosides and nucleic acids. The prevalent contemporary use of molecular modelling requires detailed knowledge of such phenomena, since molecular mechanics force fields must be specifically parametrized to take account of these effects.[5] In providing a theoretical rationale for these phenomena, explanations including hyperconjugative orbital mixing, electrostatic, steric and solvation effects have been employed, with as yet, incomplete agreement. Moreover recently, the very existence of one of these phenomena, the reverse anomeric effect has been called into question.[6]

Anomeric stabilization is a useful term that quantifies the relative stabilization of pyranose derivatives, described by the Edward–Lemieux effect (Scheme 1). Anomeric stabilization is the extra stabilization experienced by a system possessing an anomeric fragment after steric effects have been taken into account.[7] Usage is not restricted to pyranose derivatives.

anomeric stabilization = $\Delta G°$(heterocycle) − $\Delta G°$(steric) (1)

$\Delta G°$(steric) refers to a control system, which does not possess an anomeric fragment. In the specific case of pyranose

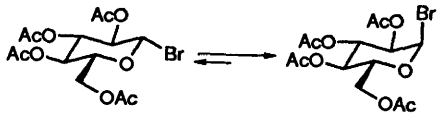

Scheme 1

derivatives, *A*-values for substituted cyclohexanes may be used, but must be corrected for structural modifications in the heterocyclic system. Unfavourable 1,3-diaxial steric interactions disfavour the axial conformer or anomer in such molecules. For the GAE to apply, anomeric stabilization of the axial isomer must be dominant over the competing steric effects. The reverse anomeric effect describes a conformational preference opposite to the GAE and in the specific case of pyranosides, the preference for the equatorial over the axial conformer, in particular where the anomeric substituent is N^+.† Experiments to support a reverse anomeric effect are not plentiful, based on conformational analysis of *N*-heterocyclic ammonium glycosides.[4] The most compelling experimental observation is of an equatorial preference for the imidazolide **1** driven by protonation (Scheme 2).[11] Since *N*-protonation is assumed to result in little steric perturbation, some special equatorial stabilization must be invoked. Implicit in the reverse anomeric effect is an *anomeric destabilization* which *in simile* with anomeric stabilization requires a further contribution, over and above simple steric effects. This destabilization in pyranose

† The term reverse anomeric effect has been defined to describe other phenomena.[8] Pinto and Leung suggest the term be reserved for systems containing quaternary nitrogen aromatic substituents,[9] in place of the more general definition employed by others.[10]

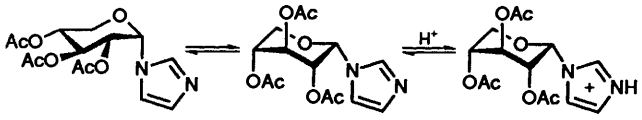

Scheme 2

derivatives favours the equatorial conformer and is also quantified by eqn. (1). The term reverse anomeric effect was coined simply to describe the phenomenon observed in *N*-heterocyclic glycosides.[4] This effect has gained added notoriety in part because the molecular orbital rationale for the GAE cannot account for the reverse anomeric effect. Thus the reverse anomeric effect has been presented as a significant inconsistency and a major flaw in the molecular orbital rationale of the GAE.[6a,12]

The reverse anomeric effect has been the focus of recent experimental studies.[6a] In addition, several recent computational studies have, in part, dealt with this effect.[9,13-15] In these studies, *N*-ammonium pyranosides or truncated acyclic models have been used to gain information on the reverse anomeric effect. The compounds under study contained primary, secondary, or tertiary ammonium anomeric substituents. However, in no case has the imidazolide system been studied, that represents the clearest experimental support for the existence of the reverse anomeric effect. Decomposition of torsional energy profiles as a computational technique has been used extensively by Deslongchamps, Grein and co-workers in studies on the anomeric effect.[15] Schleyer's group has used Weinhold's natural bond orbital (NBO) analysis[16] to good advantage in quantification of anomeric hyperconjugation.[17] Solvation approximations have been applied to semiempirical and *ab initio* calculations to estimate solvation contributions to anomeric effects.[13] In this work, we examine the effects of protonation on the conformational potential energy surfaces for *N*-pyranosylimidazolides and truncated model systems, employing *ab initio* calculations at levels up to MP2/6-31G*//RHF/6-31G*, semiempirical AM1 calculations, NBO analysis of hyperconjugation and solvation approximations using continuum dielectric models. The computational data (*i*) are in good accord with the original experimental data of Paulsen *et al.*;[11] (*ii*) reveal a rationale for the observed reverse anomeric effect and (*iii*) yield predictions as to the generality of such a phenomenon.

Methodology

The energy and structure of pyranosides **2** were obtained by geometry optimization using the AM1 Hamiltonian[18] as implemented in SPARTAN 3.0[19] on an SGI Iris Indigo. The energy and structure of conformers of the truncated model compounds **3**, **4** and **5** were calculated employing geometry optimization at the RHF/6-31G* and RHF/3-21G(*) levels using GAUSSIAN 92[20] on an IBM RISC 6000/320E or 355 or using SPARTAN 3.0, using the standard basis sets supplied.[21] The torsion angles H–C1′–O–C3′ (τ_2) and H–C3′–O–C1′ (τ_3) were fixed to mimic the properties of a pyranose ring. C2–N1–C1′–O (τ_1) was fixed at 30° increments from −180° to +180°, with full geometry optimization at each point. In one set of calculations, τ_1 was released and the torsional angle N1–C1′–O–C3′ (τ_4) was fixed incrementally between 0° and 360°, with full geometry optimization at each point. Selected torsional energy profiles and energy minima were re-calculated at the MP2(frozen core)/6-31G*//RHF/6-31G* level.[22] Energy minima obtained from torsional energy profiles were further geometry optimized (with τ_1 and τ_4 relaxed) to provide final minimum energy structures (Table 1). Structures denoted with suffixes ⊥, *cis* and *trans* correspond to optimization with fixed τ_1 at 90°, 0° and 180°, respectively. Pre-orthogonal NBO overlap matrices were obtained and second-order perturbational analyses performed with GAUSSIAN 92. Dipole moments, Mulliken charges, natural charges and charges derived from electrostatic potentials (CHELPG),[23] were recorded for each structure (Table 1). Solvation correction energies were added to both semiempirical and *ab initio* molecular energies. The continuum dielectric solvation models employed were those contained in the SPARTAN package (AM1-SM1, AM1-SM2, AM1aq.),[24] in addition to a further model developed by Lim and Chan.[25] For **3**, **4** and **5** *ab initio* geometries were used for solvation calculations. Maps of summed electrostatic and polarization potentials were calculated in SPARTAN using the HF/3-21G(*) basis set.

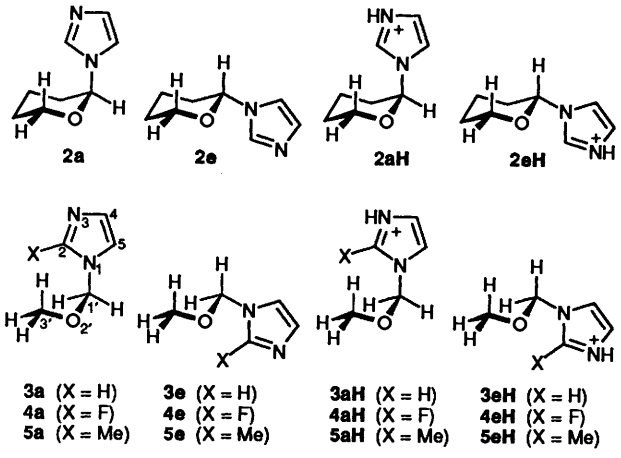

Results

Torsional Energy Profiles for Imidazolides (**3**).—In order to study the imidazolides at a reasonable level of calculation (that is, MP2/6-31G*//RHF/6-31G*), an acyclic, truncated model system was employed, in which τ_2 and τ_3 were fixed to mimic the parent cyclic pyranose system, providing **3a**, **3e**, **3aH**, and **3eH** as models of **1a**, **1e**, **1aH**, and **1eH**, respectively. Torsional energy profiles for rotation about the C–N bond for each of the four isomers of imidazolide **3** were obtained [Figs. 1(*a*)–(*d*)]. Protonation was observed to have little effect on the profiles for both axial imidazolides (**3a**, **3aH**), which, indeed, are very similar, with energy maxima at τ_1 (= τ[C_2–N–C–O]) ≈45° and −135° and minima at $\tau_1 \approx 120°$ and −60°. The maximum 1,3-diaxial interactions involving the imidazole substituent are located at $\tau_1 \approx 45°$ and −135° (Fig. 2). The calculated torsional energy profiles correspond approximately to a twofold (V_2) potential and are compatible with the dominance of the unfavourable 1,3-diaxial steric effect (Fig. 2). The amplitude of the torsional variation in energy is ≈2 kcal mol^{-1} (≈20%) greater for the unprotonated imidazolide **3a**. This is compatible with the lengthening of the C–N bond in the protonated imidazolide (**3aH**) and a reduced 1,3-diaxial interaction (Table 1). In contrast with the axial imidazolides, the equatorial isomers (**3e**, **3eH**) demonstrate strikingly different torsional energy profiles. The twofold (V_2) profile of the unprotonated imidazolide **3e** is similar to that of the axial conformers, but with energy maxima at $\tau_1 \approx 0°$ and 180° and minima at 100° and −100°. In the absence of any large 1,3-diaxial interactions, the only significant steric interaction involving the imidazole substituent is with the larger oxygen atom at $\tau_1 \approx 0°$ and 180° (Fig. 2). This interaction is minimized at $\tau_1 \approx 90°$ and −90°. As might be expected, the amplitude of the energy profile for **3e** (3 kcal mol^{-1} at HF/6-31G*) is significantly smaller than calculated for **3a** or **3aH**. The very different torsional energy profile for **3eH** appears

Table 1 Molecular energies, bond angles, bond lengths, torsion angles, charges at atoms, molecular dipoles for minimum energy and constrained isomers of **3**, **4** or **5**

Structure	**3a**		**3e**		**3aH**		**3eH**	
τ_1 (varies for 3-21G*)	−68.1°	115.3°	−95.0°	93.0°	−41.4°	131.1°	−0.15°	90.0°
Ab initio energies								
RHF/3-21G* (au)	−375.615 532	—	−375.609 919	—	−376.019 693	—	−376.023 746	—
RHF/6-31G* (au)	−377.727 149	−377.727 986	−377.725 009	−377.724 949	−378.115 284	−378.114 882	−378.117 426	−378.114 434
E_{rel}/kcal mol^{-1} [a]	0.53	0.00	1.87	1.91	1.34	1.60	0.00	1.86
MP2/6-31G*//RHF/6-31G*	−378.864 173	−378.865 188	−378.860 672	−378.860 618	−379.243 273	−379.242 963	−379.242 576	−379.240 561
E_{rel}/kcal mol^{-1} [a]	0.64	0.00	2.83	2.87	0.00	0.19	0.44	1.70
Geometry								
d(C–N)/Å	1.443	1.442	1.427	1.427	1.490	1.488	1.471	1.463
d(C–O)/Å	1.380	1.379	1.386	1.387	1.356	1.354	1.366	1.367
d(O · · · N1)/Å	2.363	2.357	2.302	2.303	2.347	2.343	2.266	2.274
d(O · · · H2)/Å	3.129	3.757	3.475	3.449	2.716	3.907	2.375	3.384
d(O · · · H5)/Å	3.727	3.077	3.265	3.291	4.067	2.826	4.102	3.276
∠OCN(°)	113.7	113.3	109.8	109.8	111.0	111.0	106.0	106.9
∠NCH2(°)	121.6	121.7	121.6	121.6	125.3	125.8	125.2	125.6
∠NCH5(°)	122.0	121.9	122.0	122.0	122.1	121.5	122.2	121.8
Charges (CHELPG/Mulliken), *e*								
N1	0.030/−0.612	0.091/−0.609	−0.067/−0.606	−0.043/−0.606	0.038/−0.621	0.040/−0.609	0.075/−0.631	−0.060/−0.595
C2	0.281/0.283	0.191/0.271	0.262/0.286	0.256/0.287	0.245/0.414	0.075/0.406	0.179/0.433	0.167/0.426
N3	−0.614/−0.524	−0.569/−0.524	−0.591/−0.526	−0.592/−0.526	−0.372/−0.702	−0.217/−0.702	−0.306/−0.712	0.203/−0.703
C4	0.241/−0.060	0.189/−0.059	0.222/−0.061	0.216/−0.061	0.036/0.022	−0.112/0.024	−0.028/0.028	−0.030/0.020
C5	−0.421/−0.014	−0.361/−0.006	−0.357/0.004	−0.354/0.004	−0.230/0.025	−0.074/0.029	−0.190/0.021	−0.141/0.042
H2	0.090/0.217	0.093/0.208	0.096/0.209	0.100/0.209	0.171/0.332	0.202/0.319	0.185/0.339	0.203/0.322
H3	—	—	—	—	0.410/0.464	0.379/0.464	0.395/0.463	0.382/0.465
H4	0.074/0.200	0.080/0.200	0.071/0.199	0.074/0.199	0.199/0.310	0.227/0.310	0.213/0.308	0.207/0.310
H5	0.198/0.217	0.201/0.227	0.204/0.220	0.201/0.220	0.226/0.302	0.205/0.315	0.220/0.300	0.234/0.305
C1′	0.177/0.189	0.069/0.191	0.314/0.221	0.255/0.220	0.266/0.198	0.225/0.191	0.175/0.264	0.350/0.208
O2′	−0.410/−0.593	−0.349/−0.594	−0.379/−0.589	−0.360/−0.589	−0.420/−0.589	−0.378/−0.577	−0.392/−0.639	−0.380/−0.592
Dipole/dynes	3.806	2.975	4.954	4.912	4.083	5.345	2.886	4.227

(continued)

Table 1 (*contd.*)

Structure	**4a**		**4e**		**4aH**		**4eH**			
τ_1 (varies for 3-21G*)	−74.7°	111.3°	−91.3°	90.8°	−66.4°	130.9°	−92.9°	96.2°	0.0°	180.0°
Ab initio energies										
RHF/3-21G* (au)	—	—	—	—	—	—	—	—	—	—
RHF/6-31G* (au)	−476.579 848	−476.581 113	−476.578 485	−476.578 491	−476.951 856	−476.952 959	−476.952 674	−476.952 690	−476.948 783	−476.951 412
E_{rel}/kcal mol^{-1} [a]	0.77	0.00	1.65	1.65	0.69	0.00	0.18	0.17	2.62	0.97
MP2/6-31G*// RHF/6-31G*	−477.879 707	−477.880 819	−477.876 772	−477.876 779	−478.242 304	−478.243 462	−478.241 231	−478.241 254	−478.236 780	−478.240 206
E_{rel}/kcal mol^{-1}	0.70	0.00	2.54	2.53	0.26	0.00	1.40	1.39	2.62	2.04
Geometry										
d(C–N)/Å	1.446	1.448	1.430	1.430	1.500	1.497	1.468	1.468	1.483	1.484
d(C–O)/Å	1.377	1.377	1.385	1.385	1.352	1.351	1.366	1.366	1.359	1.362
d(O ··· N1)/Å	2.368	2.353	2.298	2.298	2.361	2.343	2.271	2.270	2.290	2.262
d(O ··· F2)/Å	3.255	3.775	3.484	3.479	3.137	4.010	3.518	3.567	2.614	4.180
d(O ··· H5)/Å	3.670	3.137	3.310	3.314	3.763	2.842	3.229	3.177	4.074	2.410
∠OCN(°)	114.0	112.8	109.4	109.5	111.9	110.6	106.5	106.4	107.3	105.3
∠NCF2(°)	119.1	119.2	119.1	119.1	124.8	124.9	124.8	124.8	127.5	124.3
∠NCH5(°)	121.8	121.6	121.7	121.7	121.4	120.9	121.2	121.2	121.2	120.9
Charges (CHELPG/Mulliken), *e*										
N1	−0.052/−0.673	0.006/−0.670	−0.157/−0.667	−0.174/−0.668	−0.083/−0.671	−0.052/−0.669	−0.147/−0.651	−0.139/−0.651	−0.039/−0.690	−0.068/−0.685
C2	0.709/0.907	0.636/0.890	0.702/0.907	0.702/0.907	0.664/1.072	0.538/1.051	0.645/1.072	0.629/1.071	0.646/1.081	0.614/1.062
N3	−0.657/−0.572	−0.622/−0.569	−0.634/−0.572	−0.632/−0.572	−0.406/−0.755	−0.308/−0.752	−0.370/−0.754	−0.362/−0.754	−0.409/−0.761	−0.390/−0.755
C4	0.204/−0.052	0.165/−0.056	0.173/−0.056	0.163/−0.056	−0.027/0.025	−0.135/0.024	−0.038/0.022	−0.038/0.022	−0.028/0.033	−0.080/0.016
C5	−0.465/−0.018	−0.430/−0.005	−0.391/0.002	−0.373/0.002	−0.212/0.026	−0.102/0.030	−0.180/0.045	−0.182/0.045	−0.220/0.018	−0.132/0.048
F2	−0.228/−0.341	−0.236/−0.350	−0.227/−0.346	−0.227/−0.346	−0.131/−0.256	−0.124/−0.265	−0.123/−0.262	−0.120/−0.262	−0.136/−0.247	−0.141/−0.269
H3	—	—	—	—	0.420/0.474	0.403/0.474	0.409/0.474	0.407/0.474	0.421/0.472	0.423/0.473
H4	0.105/0.212	0.108/0.211	0.105/0.211	0.108/0.211	0.226/0.317	0.248/0.316	0.224/0.316	0.223/0.316	0.229/0.315	0.235/0.314
H5	0.226/0.224	0.234/0.233	0.226/0.227	0.219/0.227	0.240/0.308	0.224/0.320	0.257/0.312	0.256/0.312	0.238/0.307	0.220/0.328
C1′	0.208/0.189	0.160/0.182	0.366/0.216	0.401/0.216	0.232/0.182	0.267/0.186	0.323/0.204	0.337/0.204	0.218/0.269	0.270/0.266
O2′	−0.424/−0.588	−0.366/−0.592	−0.372/−0.591	−0.385/−0.591	−0.395/−0.570	−0.385/−0.575	−0.368/−0.594	−0.368/−0.594	−0.368/−0.622	−0.344/−0.627
Dipole/dyne	4.574	3.058	5.084	5.075	4.842	4.182	3.622	3.601	4.014	2.949

Table 1 (*contd.*)

Structure	**5a**		**5e**	**BaH′**	**5aH**	**5eH**			
τ_1 (varies for 3-21G*)	119.4°	−70.3°	−80.5°	134.4°	−64.3°	−69.6°	69.4°	0.0°	−90.0°
Ab initio energies									
RHF/3-21G* (au)	—	—	—	—	—	—	—	—	—
RHF/6-31G*(au)	−416.769 088	−416.770 065	−416.767 811	−417.164 122	−417.165 862	−417.165 609	−417.165 605	−417.162 522	−417.164 981
E_{rel}/kcal mol^{-1}	0.61	0.00	1.41	1.09	0.00	0.16	0.16	2.10	0.55
MP2/6-31G*//RHF/6-31G*	−418.038 307	−418.039 430	−418.035 819	−418.423 278	−418.425 157	−418.423 267	−418.423 253	−418.419 432	−418.422 2951
E_{rel}/kcal mol^{-1}	0.70	0.00	0.89	1.18	0.00	1.19	1.19	3.59	1.80
Geometry									
d(C–N)/Å	1.444	1.442	1.427	1.484	1.482	1.460	1.460	1.473	1.458
d(CO)/Å	1.380	1.381	1.387	1.357	1.360	1.371	1.371	1.364	1.370
d(O • • • N1)/Å	2.351	2.363	2.305	2.340	2.359	2.281	2.281	2.301	2.277
d(O • • • C6)/Å	4.091	3.345	3.478	4.236	3.230	3.256	3.254	2.763	3.607
d(O • • • H5)/Å	2.974	3.675	3.448	2.741	3.753	3.583	3.584	4.042	3.276
d(O • • • H6)/Å	3.830	2.822	2.992	4.031	2.621	2.715	2.718	2.581	3.137
∠OCN(°)	112.7	113.6	109.9	110.8	112.1	107.3	107.3	108.3	107.2
∠NCC6(°)	124.2	123.2	123.3	127.5	126.7	126.7	126.7	130.3	126.9
∠NCH5(°)	121.7	122.0	121.9	121.4	121.9	121.8	121.8	121.7	121.7
Charges (CHELPG/Mulliken), *e*									
N1	0.039/−0.658	−0.041/−0.655	−0.173/−0.655	−0.002/−0.666	−0.015/−0.663	−0.098/−0.654	−0.104/−0.654	0.083/−0.688	−0.104/−0.648
C2	0.413/0.545	0.521/0.556	0.535/0.562	0.331/0.685	0.435/0.694	0.420/0.705	0.428/0.704	0.507/0.695	0.431/0.702
N3	−0.625/−0.562	−0.657/−0.561	−0.635/−0.563	−0.304/−0.748	−0.395/−0.747	−0.331/−0.749	−0.344/−0.749	−0.351/−0.749	−0.342/−0.750
C4	0.174/−0.060	0.169/−0.059	0.169/−0.062	−0.113/0.020	−0.012/0.019	−0.073/0.017	−0.075/0.017	0.101/0.027	−0.046/0.017
C5	−0.393/−0.004	−0.425/−0.015	−0.344/0.002	−0.112/0.028	−0.215/0.024	−0.141/0.037	−0.127/0.036	−0.348/0.018	−0.161/0.042
C6	−0.393/−0.551	−0.250/−0.553	−0.267/−0.555	−0.298/−0.557	−0.281/−0.562	−0.319/−0.560	−0.309/−0.560	−0.515/−0.513	−0.324/−0.561
H3	—	—	—	0.386/0.454	0.403/0.455	0.391/0.455	0.397/0.455	0.348/0.454	0.391/0.455
H4	0.090/0.197	0.089/0.198	0.090/0.197	0.229/0.304	0.209/0.304	0.218/0.304	0.219/0.304	0.167/0.303	0.210/0.304
H5	0.212/0.225	0.204/0.212	0.200/0.215	0.216/0.310	0.225/0.296	0.224/0.298	0.219/0.298	0.252/0.294	0.238/0.300
C1′	0.118/0.190	0.146/0.190	0.371/0.222	0.242/0.192	0.184/0.183	0.317/0.215	0.291/0.216	0.035/0.265	0.304/0.207
O2′	−0.378/−0.595	−0.413/−0.597	−0.392/−0.593	−0.391/−0.581	−0.387/−0.584	−0.385/−0.602	−0.379/−0.602	−0.421/−0.633	−0.382/−0.595
Dipole/dyne	3.192	3.696	4.839	4.717	3.857	3.259	3.243	2.595	3.604

[a] Energy relative to the minimum-energy conformer for each imidazolide: **3**, **4** or **5**.

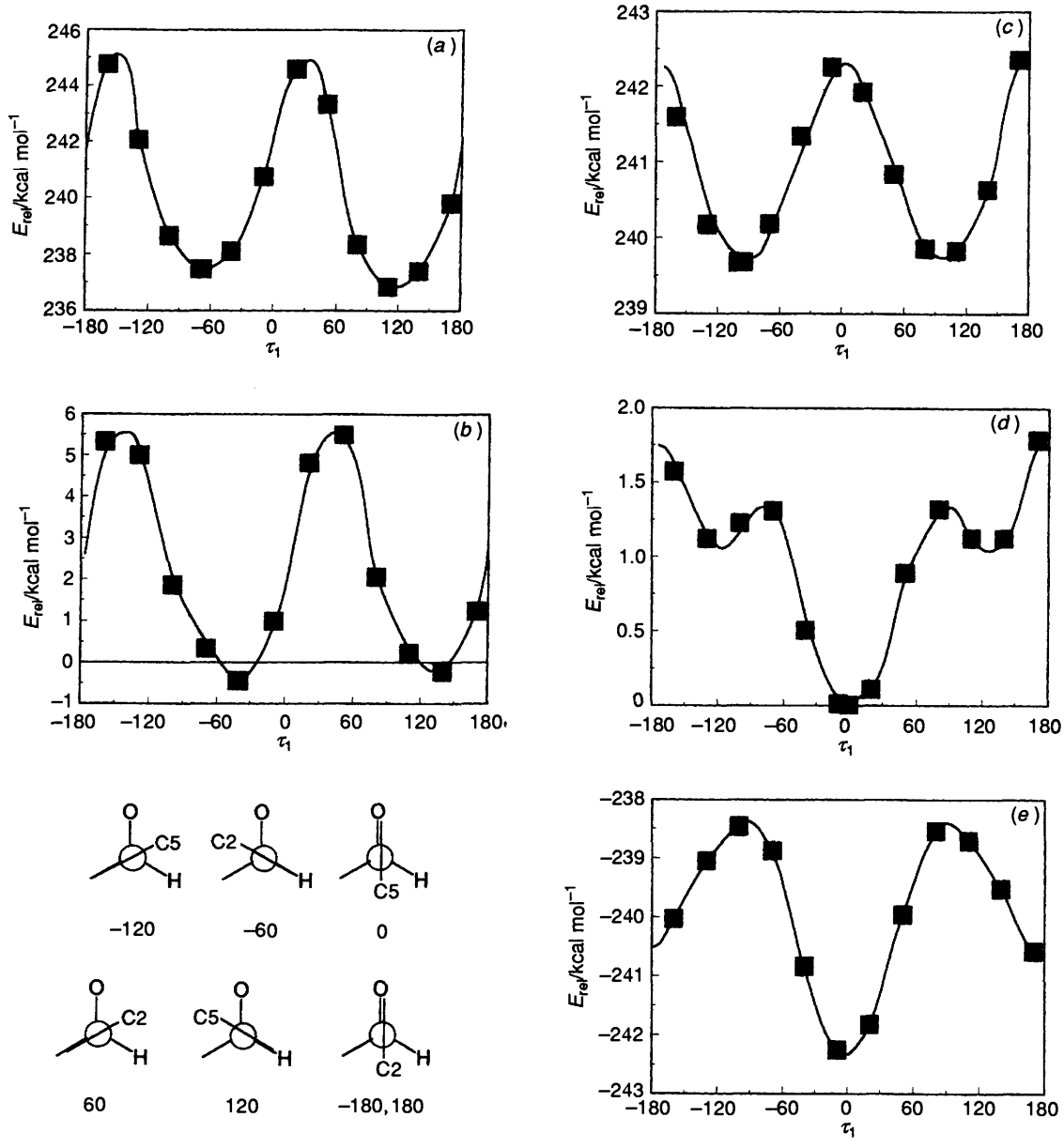

Fig. 1 Torsional energy profiles for rotation about N1–C1′ bond of imidazolides: (*a*) **3a**; (*b*) **3aH**; (*c*) **3e**; (*d*) **3eH**. All energies relative to minimum-energy conformer of **3eH**, calculated at the MP2/6-31G*//RHF/6-31G* level. (*e*) Difference energy profile: *E*(**3eH**) − *E*(**3e**). Structures show Newman projections along N1–C1′ with corresponding values of τ_1.

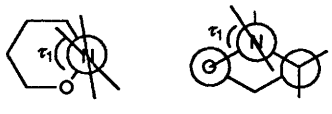

Fig. 2 Newman projection along N1–C1′, for axial imidazolides (left) and equatorial imidazolides (right), showing rotamers with steric interactions minimized and corresponding τ_1

dominated by a V_1 potential superimposed on the same V_2 potential that dominates the torsional energy of **3e**. The energy minimum is at $\tau_1 \approx 0°$, which is an energy maximum for the unprotonated equatorial imidazolide **3e**. The energy maximum is at $\tau_1 \approx 180°$. Again, the amplitude of the energy change (3 kcal mol^{-1} at HF/6-31G*) is small for the equatorial imidazolides. The data for **3eH** clearly indicate the influence of what appears to be a stabilizing V_1 contribution with an optimum interaction at $\tau_1 \approx 0°$, when the C2 of the imidazole and oxygen are eclipsed. The size of this stabilizing effect can be estimated from subtraction of the steric interactions, using the torsional profile for **3e**. The resultant profile shows a stabilization of about 4 kcal mol^{-1} at $\tau_1 \approx 0°$ and moreover, a smaller stabilization of $\approx$2 kcal mol^{-1} at $\tau_1 \approx 180°$ [Fig. 1(*e*)]. Thus the torsional energy profiles for the imidazolides **3a**, **3e**, **3aH**, **3eH** can be rationalized by destabilizing steric interactions of 3–9 kcal mol^{-1} and the presence of an unascribed stabilizing contribution, which dominates the profile of the protonated equatorial imidazolide **3eH**, with a maximal value of 4 kcal mol^{-1}.

Torsional Energy Profiles for 2-Fluoroimidazolides (**4**).—The protonated 2-fluoroimidazole congeners of **3aH** and **3eH** are **4aH** and **4eH**, respectively. The twofold torsional energy profile for **4aH** is similar in amplitude and form to that of **3aH**, with energy maxima and minima occurring at very similar torsional angles [Fig. 3(*a*), (*b*)]. The single difference is dissymmetry introduced by substitution of fluorine for hydrogen at the 2-position of **4aH**, leading to unfavourable 4e$^-$ and dipole interactions between F and O at $\tau_1 \approx 45°$ and raising this energy maximum. The torsional profile for rotation about the N–C bond of **4eH**, conversely, is quite

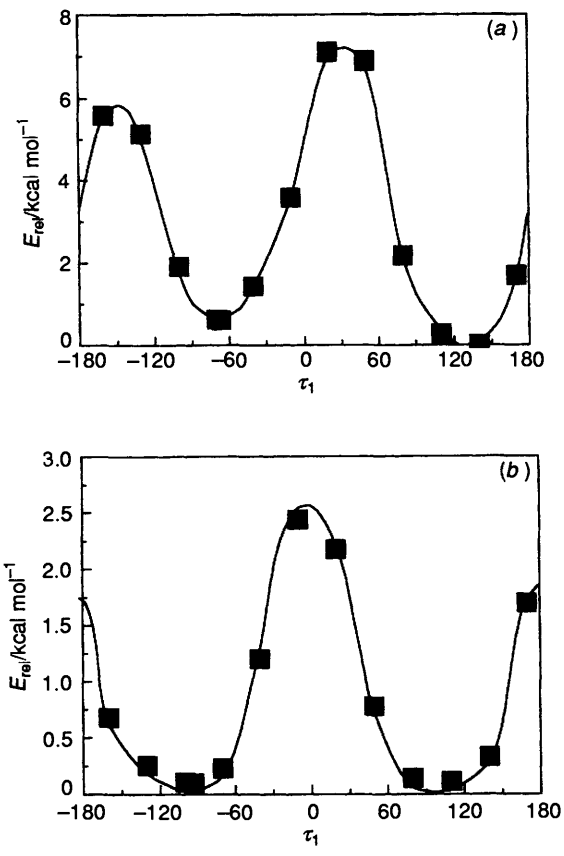

Fig. 3 Torsional energy profiles for rotation about N1–C1′ bond of 2-fluoroimidazolides: (*a*) **4aH**; (*b*) **4eH**. All energies relative to minimum energy conformer of **4eH**, calculated at MP2/6-31G*//RHF/6-31G*.

unlike that calculated for **3eH**. The energy profile is, in fact, very similar to that for **3e**, with minima and maxima at similar torsional angles and a similarly small amplitude. Whatever stabilizing contribution influences the torsional profile for **3eH**, is absent in the energy profile calculated for its 2-fluoro congener **4eH**.

Torsional Dependence of Bond Lengths and Angles.—The torsional dependence on rotation about the C–N bond of **3a** suggests that lengthening of the C–N bond is correlated with contraction of the C–O bond [Fig. 4(*a*)]. This is compatible with the GAE, but more probably results from the 1,3-diaxial steric interaction, since the maximum C–N bond lengthening ($\approx$0.02 Å) occurs at $\tau_1 \approx 20°$ and $-160°$ corresponding to the torsional energy maxima. The torsional bond length dependence for **3e**, similarly, shows correlation of the C–N and C–O bond lengths with the C–N bond increased ($\approx$0.015 Å) to minimize steric interactions at the energy maxima. The bond length dependence for both protonated imidazolides is more complex [Fig. 4(*c*), (*d*)]. C–N Bond lengthening and C–O shortening at the energy maxima for **3aH** and **3eH** is compatible with minimization of unfavourable steric interactions [Fig. 4(*c*), (*d*)]. However, at torsion angles close to $\tau_1 \approx 0°$, the correlated C–N bond lengthening and C–O shortening breaks down. The torsional dependencies of C–N and C–O bond lengths for the 2-fluoroimidazolides **4aH** and **4eH** are compatible with lengthening of the C–N bond to minimize steric interactions together with a concomitant shortening of the C–O bond [Fig. 5(*a*), (*b*)]. This relationship is more akin to the unprotonated than protonated imidazolides **3**.

Axial imidazolides **3a** and **3aH** are expected to demonstrate significant bond length and angle changes associated with the presence of the GAE.[1] An optimal GAE corresponds to widening of the bond angle at the anomeric centre. However, the opening of the bond angle at the anomeric centre by 6° on

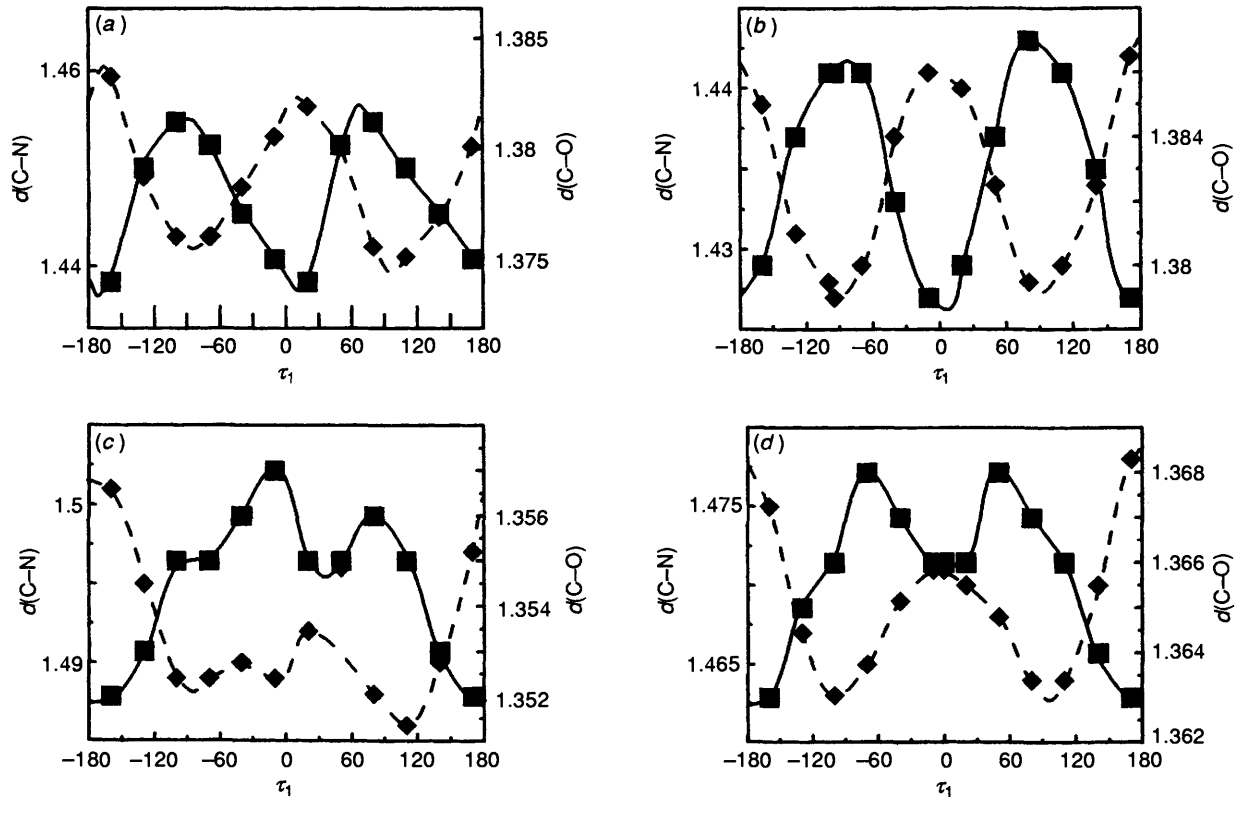

Fig. 4 Torsional dependence of N1–C1′ (– – – –) and C1′–O2′ (——) bond lengths (Å) on rotation about N1–C1′ bond for (*a*) **3a**; (*b*) **3aH**; (*c*) **3e**; (*d*) **3eH**

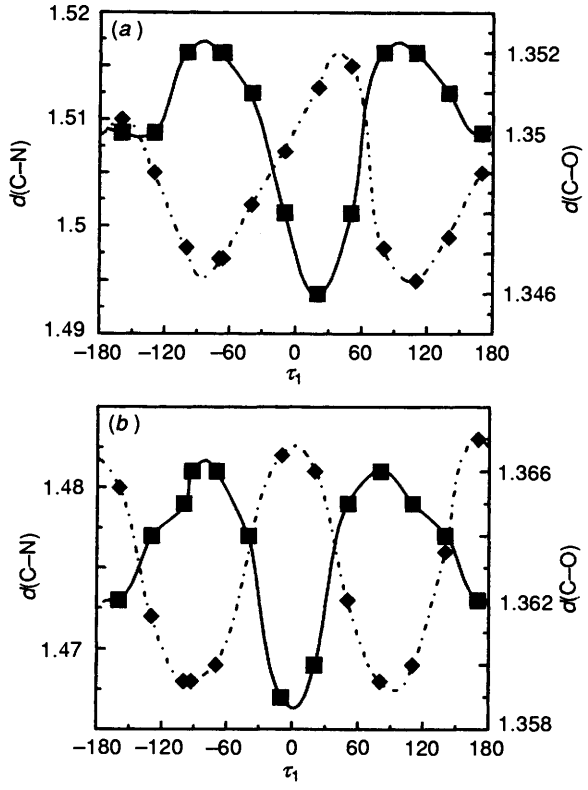

Fig. 5 Torsional dependence of N1–C1′ (– – – –) and C1′–O2′ (——) bond lengths (Å) on rotation about the N1–C1′ bond for (*a*) **4aH**; (*b*) **4eH**

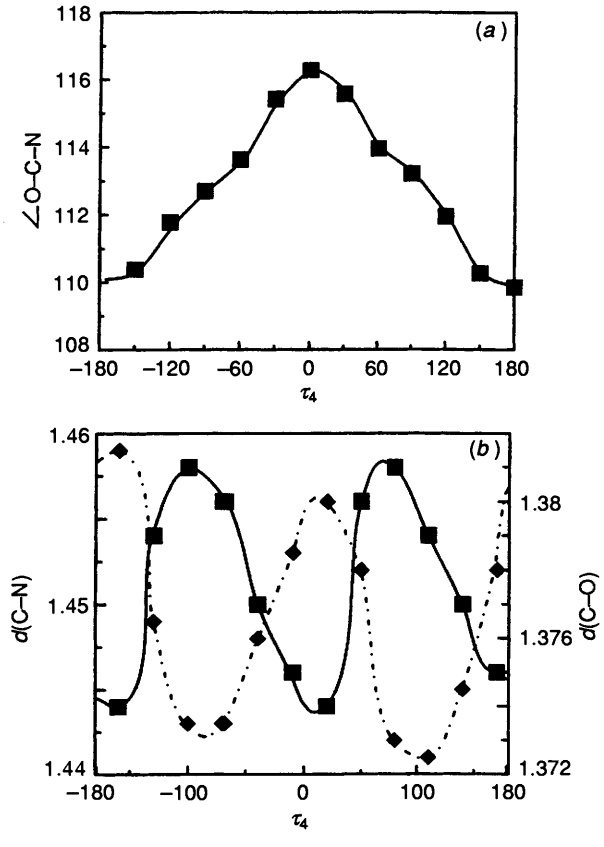

Fig. 6 Torsional dependence of O2′–C1′–N1 bond angle and N1–C1′ (– – – –) and C1′–O2′ (——) bond lengths (Å) on rotation about the O2′–C1′ bond for **3aH**

rotating about the C–O bond from $\tau_4 = 180°$ to $\tau_4 = 0°$ is also compatible with minimization of unfavourable steric

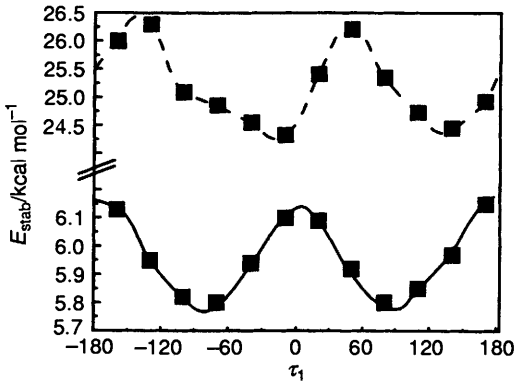

Fig. 7 Torsional dependence of n(O)→σ*(C–N) stabilization energies for **3aH** (– – – –) and **3eH** (——) from summed pairwise interactions in second orbital perturbational NBO analysis (HF/6-31G*)

interactions [Fig. 6(*a*)]. Evidence for the presence of the GAE is shown in the correlated C–N and C–O bond length changes on rotation about the C–O bond [Fig. 6(*b*)]. The maximum elongation of the C–N bond at $\tau_1 \approx 60°$ corresponds to the maximal GAE and not reduction of steric interactions.

Natural Bond Orbital Analysis.—The torsional dependence of the second-order perturbational interaction energies was recorded for each conformer of the imidazolides **3aH**, **3eH**. The chief purpose was examination of stabilizing interactions involving n(O) as electron donor. No interactions (> 0.5 kcal mol^{-1}) were observed with acceptor orbitals localized on the C–H bonds of the imidazole ring. The expected n(O)→σ* (C–N) anomeric hyperconjugation was observed and some dependence on τ_1 was evident (Fig. 7). The presence of a smaller anomeric hyperconjugation in the equatorial imidazolides (**3e**, **3eH**) is not unexpected. The magnitude of stabilization decreases **3aH** > **3a** > **3eH** > **3e** (24, 18, 6, 4 kcal mol^{-1}, respectively) in accord with expectations based upon reduced orbital overlap in the equatorial isomers and a lowering in energy of the acceptor σ* orbital on *N*-protonation. Increased n(O)→σ*(C–N) stabilization is observed for **3aH** at values of τ_1 corresponding to overall energy maxima, whereas increased n(O)→σ*(C–N) stabilization is observed for **3eH** at values of τ_1 corresponding to overall energy minima. The torsional dependence of anomeric hyperconjugation therefore opposes the dominant steric effects in **3aH**, but reinforces the stabilizing interaction observed in the torsional profile of **3eH**, although the magnitude of hyperconjugation is small in the latter case.

Charges at Atoms and Electrostatic Interactions.—Calculated Mulliken, natural and electrostatic charges indicate that protonation of the imidazole nitrogen increases the acidity of all protons on the imidazole ring. Rotation about the C–N bonds of **3aH** and **3eH** brings H2 of the imidazole ring to within 2.65 Å and 2.38 Å and H5 to within 2.57 Å and 2.40 Å of oxygen, respectively. The simple coulombic contribution to potential energy was calculated as a function of τ_1 for **3aH**, **3a**, **3eH** and **3e** using Mulliken, natural and electrostatic charges at H2, H5 and O. Torsional profiles are qualitatively identical regardless of the charge type employed in the calculation. Overlap of H5 with O at $\tau_1 \approx 180°$ yields electrostatic stabilization energies of 17, 18, 24 and 27 kcal mol^{-1} for **3a**, **3e**, **3aH** and **3eH**, respectively, from Mulliken charges [Fig. 8(*a*)]. Overlap of H2 with O at $\tau_1 \approx 0°$ yields greater electrostatic stabilization of 17, 19.5, 26 and 30.5 kcal mol^{-1} for **3a**, **3e**, **3aH** and **3eH**, respectively, from Mulliken charges [Fig. 8(*b*)]. The amplitude of the electrostatic stabilization energy is also greater for the interaction involving H2 than that involving H5. Summation of

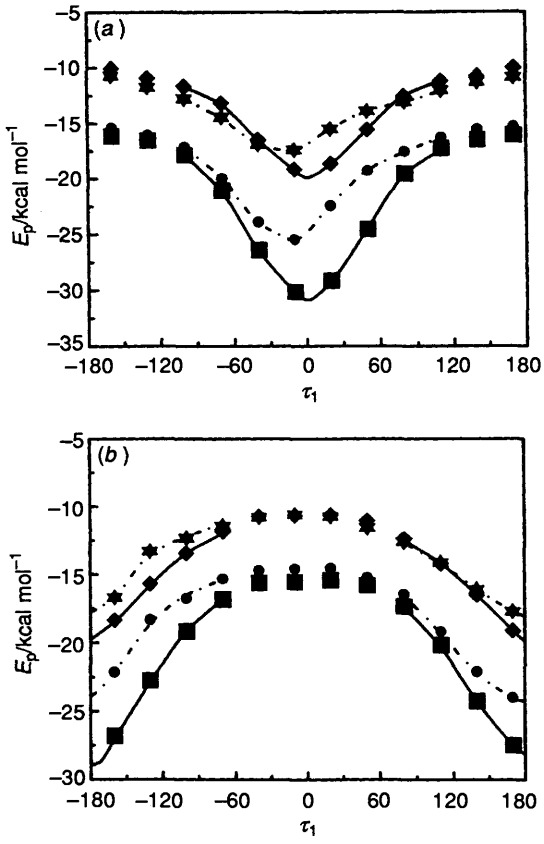

Fig. 8 Electrostatic potential-energy profiles calculated from atomic distances and atomic charges (Mulliken, at HF/6-31G*) for interaction of (*a*) O2′ with H2; (*b*) O2′ with H5; **3a** (★), **3e** (◆), **3aH** (●), **3eH** (■)

the coulombic stabilization profiles for **3eH** corresponds approximately to the energy difference profile calculated for **3eH** [Fig. 1(*e*)]. This analysis suggests that the dominant influence on the torsional energy profile of **3eH** is a stabilizing H2 • • • O hydrogen-bond, manifested in the electrostatic interaction between H2 and oxygen. In the neutral imidazolides the total charge on the imidazole ring atoms is −0.697 and −0.643 in **3a** and **3e**, respectively, employing Mulliken charges. The effect of *N*-protonation is to increase the total charge on the atoms of the imidazole ring to +0.546 and +0.592 in **3aH** and **3eH**⊥, respectively. The protonated equatorial conformer carries greater positive charge on the ring and this additional charge is concentrated most highly at H3 and C2 (Table 1). Thus the H2 • • • O hydrogen bond stabilization in **3eH** would be augmented by interaction between O and C2, the latter carrying a significant positive charge on *N*-protonation. Indeed, NBO analysis of the minimum energy conformer of **3eH** reveals a small (1 kcal mol^{-1}) n(O)→σ^*(C2–N3) charge-transfer stabilization.

Solvation Approximations.—A variety of continuum dielectric solvation models were used to calculate torsional dependence of solvation correction energies for **3a**, **3e**, **3aH** and **3eH** using the aqueous solvation algorithms, AM1-SM1, AM1-SM2 and AM1(aqueous), and HF/6-31G* optimized geometries. A further continuum dielectric model (CDM) was employed using HF/6-31G* optimized geometries. The aqueous solvation energies, derived from these methods, for the unprotonated imidazolides **3a** and **3e** are dependent on τ_1, but the amplitude is only ≈1 kcal mol^{-1} [Fig. 9(*a*), (*b*)]. The amplitude of the aqueous solvation energy for the protonated imidazolides, **3eH** and **3aH**, is ≈2 kcal mol^{-1}, with a relative destabilization of the $\tau_1 \approx 0°$ conformers [Fig. 9(*c*), (*d*)]. The

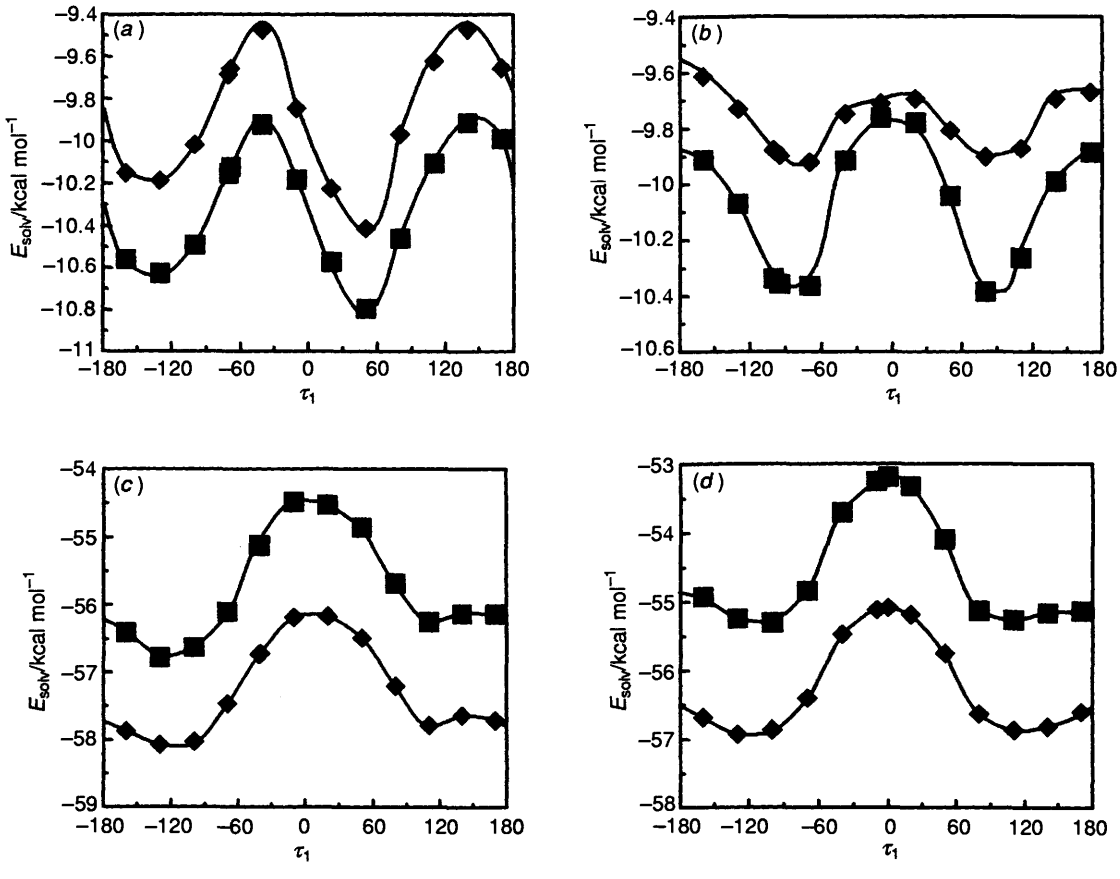

Fig. 9 Torsional dependence of aqueous solvation energies for (*a*) **3a**; (*b*) **3e**; (*c*) **3aH**; (*d*) **3eH**. AM1-SM1 (◆) and AM1-SM2 (■) calculations using HF/6-31G* geometries.

effect of aqueous solvation on the torsional energy profile for **3eH** is a relative stabilization of the conformers corresponding to energy maxima and destabilization of the energy minima, which would lead to a very shallow torsional profile for **3eH** in polar and aqueous solution and a negation of the influence of the hydrogen bond at $\tau_1 \approx 0°$.

Solvation Effects on Conformational Equilibria.—Several recent papers have dealt with the complexity of modelling solvation effects on the GAE, in particular in hydrogen bonding solvents.[14,26] In this paper, we simply employ the aqueous solvation corrections, which incorporate a high dielectric constant, to provide a model for conformational equilibria in polar solvents. This allows comparison with conformational equilibria in non-polar solvent, which are modelled by relative energies in the gas phase. The calculated data then provide a measure of the shift in equilibrium on moving from non-polar to polar solvents. For each conformer, the geometry used was that obtained in the gas phase, for **2** at the AM1 level and for **3** *ab initio* at the HF/6-31G* level. No further geometry optimization within any specifically defined solvent environment was attempted. We have defined ΔE_e as E_{calc}(eq) − E_{calc}(ax); a negative value reflecting an equatorial preference. Comparison of ΔE_e values leads to two important parameters: (1) $\delta\Delta E_{H^+}$, the effect of protonation on the conformational equilibria (Tables 2, 3); and (2) ΔE_S and $\delta\Delta E_S$, the effect of increased solvent polarity on the conformational equilibria (Table 2). Negative values reflect a shift in the equilibrium towards the equatorial conformer. Clearly, $\delta\Delta E_{H^+}$ in non-polar solvents, calculated for the isomers of imidazolide **3**, is negative regardless of the basis set employed, reflecting a relative stabilization of the equatorial isomer, on protonation, of 2.4 to 6.1 kcal mol^{-1}. The calculated values of ΔE_s and $\delta\Delta E_S$, using SM1, SM2, AM1aq. or CDM solvation models, indicate that an increase in solvent polarity leads to a shift towards the equatorial conformer for the unprotonated imidazolides, but a shift towards the axial conformer for the protonated imidazolides (Table 2). The calculated values of ΔE_S correlate with the changes in calculated total molecular dipole moments (Table 1).

Conformational and Solvation Energies of N-*Pyranosylimidazolides* (**2**).—Semiempirical calculations on the intact *N*-pyranosylimidazolides (**2**) were employed to assist in constructing the truncated models, in addition to providing a test of the truncated models in accurately reflecting properties of the intact cyclic system. The torsional dependence of SM1 and SM2 solvation energies for **2a**, **2e**, **2aH** and **2eH** is very similar to that shown for the corresponding isomers of **3** (Fig. 9) and relative values of $\delta\Delta E_S$ for **2** correspond to those calculated for **3** suggesting that the truncated model retains the ability accurately to reflect solvation effects. Furthermore, torsional energy profiles for the isomers of **2** calculated at the AM1 level (Fig. 10) are very similar to those calculated for the truncated model **3** (Fig. 1) and reflect the special stabilization of the protonated equatorial isomer at $\tau_1 = 0°$.

Structure and Energy of 2-*Fluoroimidazolides* (**4**).—Torsional profiles for the protonated 2-fluoroimidazolides resemble those for the unprotonated imidazolides, **3a**, **3e** (*vide supra*). The strong influence of the H2 · · · O hydrogen bond seen in **3eH** is not possible in **4eH**. Moreover this stabilizing interaction is replaced by a destabilizing 4e$^-$ interaction between n(O) and n(F) at $\tau = 0°$. The torsion angles, τ_1, corresponding to the minimum energy structures of **4eH** and **4aH** are very similar to those for **4e** and **4a**, respectively, and correspond to minimization of unfavourable steric interactions. The lack of the H2 · · · O hydrogen bond in **4eH** allows relaxation of the unfavourable steric interaction at $\tau_1 \approx 0°$. The energy minima for **4e** and **4eH** have the imidazole ring approximately

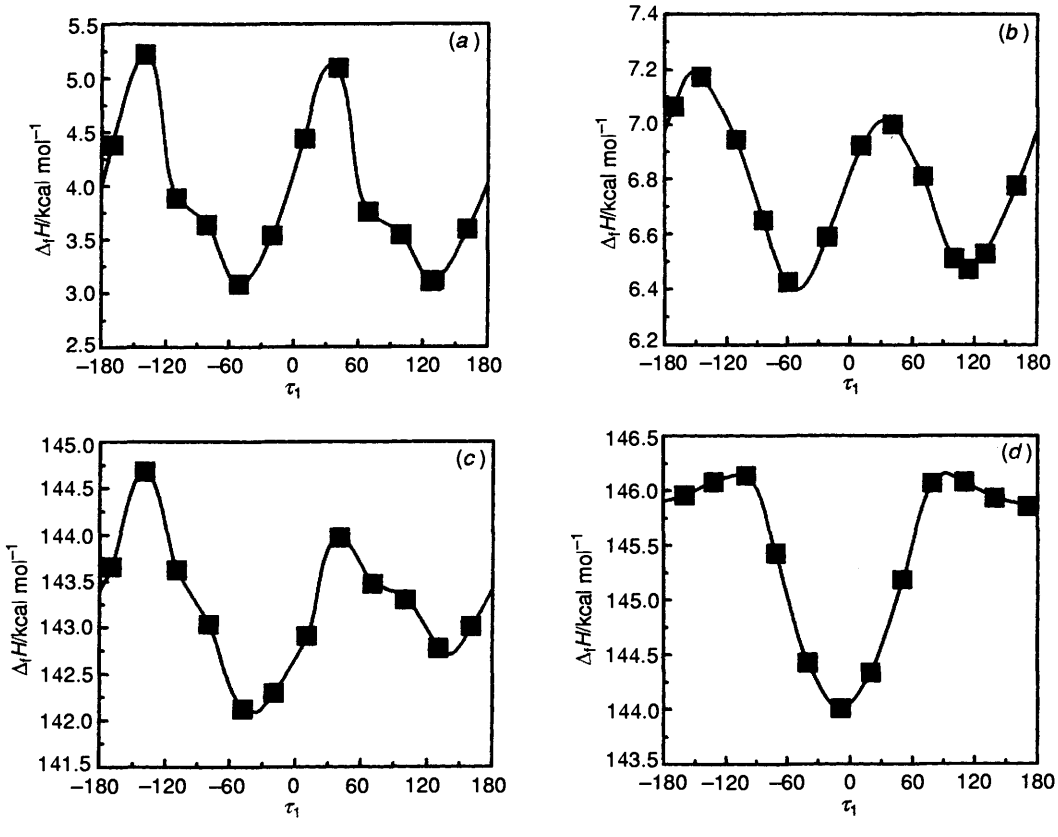

Fig. 10 Torsional energy profiles for rotation about N1–C1′ bond of imidazolides: (*a*) **2a**; (*b*) **2e**; (*c*) **2aH**; (*d*) **2eH**. Heats of formation from geometry optimization using the AM1 Hamiltonian.

Table 2 Energy differences, solvation energies and equilibrium shifts for isomers of imidazolide **3**

	Level of calculation[a]			Solvation corrections added[b]					Solvation effects	
	3-21G(*)	6-31G*	MP2	HF + CDM	MP2 + CDM	HF + SM2	MP2 + SM2		CDM	SM2
ΔE_e(**3a,3e**)	+3.52	+1.87	+2.83	+1.2	+2.1	+1.6	+2.6	ΔE_S(**3a,3e**)	−0.70	−0.24
ΔE_e(**3aH,3eH**)	−2.54	−1.34	+0.44	−0.1	+1.7	+0.3	+2.1	ΔE_S(**3aH,3eH**)	+1.27	+1.66
ΔE_e(**3aH,3eH**⊥)	+2.90	+0.52	+1.70	—	—	—	—	—	—	—
$\delta\Delta E_{H^+}$(**3**)	−6.06	−3.21	−2.39	−1.3	−0.4	−1.3	−0.5	$\delta\Delta E_S$(**3**)	+2.0	+1.9
$\delta\Delta E_{H^+}$(**3**⊥)	−0.62	−1.35	−1.13	—	—	—	—	—	—	—

$\Delta E_e = E(\text{eq}) - E(\text{ax})$; $\delta\Delta E_{H^+} = \Delta E_e(\text{protonated}) - \Delta E_e(\text{unprotonated})$, *i.e.*, the shift in equilibrium towards the equatorial conformer on protonation; $\Delta E_s = E_{solv}(\text{eq}) - E_{solv}(\text{ax})$; $\delta\Delta E_s = \Delta E_s(\text{protonated}) - \Delta E_s(\text{unprotonated})$, *i.e.*, the shift in equilibrium towards the equatorial conformer on moving from non-polar solvent (modelled by gas phase) to polar solvent (modelled by aq. solvation). [a] MP2 refers to MPS(frozen core)/6-31G*//RHF/6-31G*. [b] CDM and SM2 are the solvation algorithms of Lim and Chan and Cramer and Truhlar, respectively; HF refers to RHF/6-31G* energies.

Table 3 Conformational energy differences and shifts in equilibria for isomers of imidazolides **3**, **4** and **5**[a]

	(**3a,3e**)	(**3aH,3eH**)	(**3aH,3eH**⊥)	(**4a,4e**)	(**4aH,4eH**)	(**4aH,4eH***cis*)	(**5a,5e**)	(**5aH,5eH**)	(**5aH,5eH***cis*)	(**5aH,5eH**⊥)	(**5aH′,5eH**)
ΔE_e(HF)	+1.87	−1.34	+0.52	+1.65	+0.17	+2.62	+1.41	+0.16	+2.10	+0.55	−0.93
ΔE_e(MP2)	+2.83	+0.44 + 3.21	−1.70 + 1.35	2.53	+1.39	+4.19	+0.89	+1.19	+3.59	+1.79	+0.01
$\delta\Delta E_{H^+}$(HF)	—	−2.39	−1.13	—	−1.48	+0.97	—	−1.25	+0.69	−0.86	−2.34
$\delta\Delta E_{H^+}$(MP2)	—	–		—	−1.14	+1.66	—	+0.30	+2.70	+0.60	−0.88

[a] ΔE_e and $\delta\Delta E_{H^+}$ are defined in Table 2; negative values of $\delta\Delta E_{H^+}$ indicate a shift in equilibrium towards the equatorial conformer. HF refers to RHF/6-31G*; MP2 refers to MP2(frozen core)/6-31G*//RHF/6-31G*. Isomer notations and detailed energies are given in Table 1.

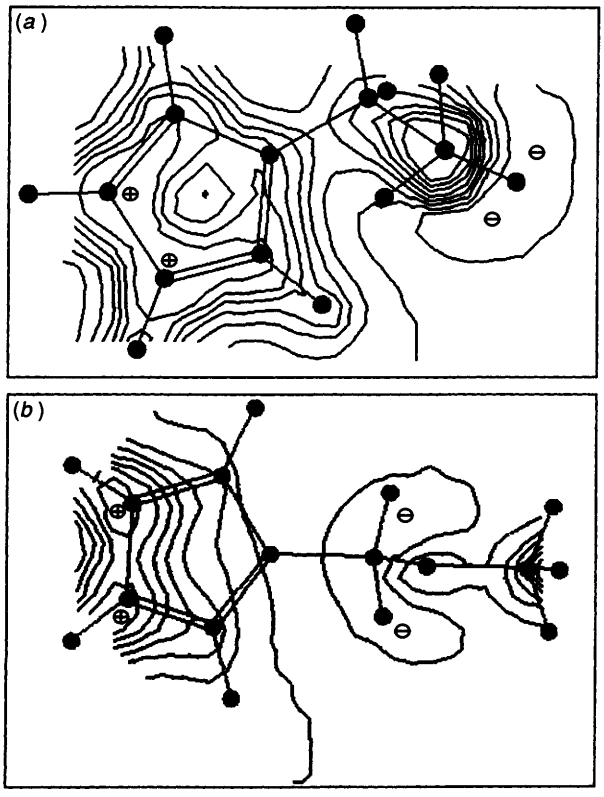

Fig. 11 Contour maps of electrostatic potential plus polarization potential for imidazolides (*a*) **3aH** and (*b*) **3eH**⊥. Negative signs indicate approximate position of maximum negative summed potential, corresponding to non-bonding electrons associated with oxygen. Positive signs indicate approximate positions of maximum summed positive potential, corresponding to positively charged imidazole ring components. To illustrate both features, the plane in (*a*) is drawn approximately through O2′, H3 and H4, whereas for (*b*) the plane is defined by H3′, H3 and H4. In (*a*) C3′ is superimposed directly upon O2′.

orthogonal to the C1′–O bond. However, the unavailability of hydrogen-bond stabilization in **4eH** does not lead to loss of the overall stabilization of the equatorial conformer on protonation. The relative equatorial stabilization on protonation, $\delta\Delta E_{H^+}$ = 1.17 kcal mol^{-1} (at the MP2 level), is smaller for **4** than for **3**, but is in the same direction. It would seem that protonation favours the equatorial imidazolide with or without the presence of the H2 ··· O hydrogen-bond. Thus in relative energy, **4eH** is stabilized over **4aH** to a greater extent than **4e** is stabilized over **4a**. Second-order perturbational NBO analysis of the energy minima for **4** does not reveal any significant, stabilizing interactions that might account for the relative conformational preference for **4eH**. However, examination of electrostatic (plus polarization) potential maps for the conformers of **4** and **3** (Fig. 11), clearly show that for the equatorial conformer, the centre of electron density associated with the non-bonding electrons on oxygen is aligned for a favourable electrostatic interaction with the face of the positively charged imidazolium ring, whereas such an interaction is not possible in the axial conformation (Fig. 11). Compatible with this interaction is the compression of the O–C–N bond angle by 6° on protonation of **4e**.

Structure and Energy of 2-Methylimidazolides (**5**).—The influence of the H2 ··· O hydrogen-bond is again obviated in **5** and as in **4**, replaced by an unfavourable interaction at τ = 0°, which in this case is steric. However, the 2-methyl substituent is expected to introduce complications if the methyl protons are sufficiently acidic to promote a stabilizing interaction with oxygen. From the above discussion, a methyl-H ··· O hydrogen-bond is likely to have most influence in the equatorial conformation in concert with *N*-protonation increasing the acidity of the methyl hydrogens. The minimum-energy conformer of **5eH** is located at τ = −69.8°, more than 20° from that located for **4eH** (Table 1). The change in torsion angle is interpreted to result from the influence of the methyl-H ··· O interaction. Furthermore, the conformer of **5aH** with the methyl group proximal to oxygen is 1.2 kcal mol^{-1} lower in energy than the alternative conformer **5aH′** (Table 1). This relatively large conformational stabilization suggests that an attractive electrostatic interaction between oxygen and the methyl hydrogens is present in **5aH**, although prevented in **3aH** for steric reasons.

Contributions to Conformational Energy of **3**, **4** *and* **5**.—The analysis above indicates that conformational energy is composed of several individual contributions. It is informative to examine values of $\delta\Delta E_{H^+}$ not only for the calculated global minimum conformations, but also for conformations with fixed τ_1 in which individual contributions are 'switched off'. The value of $\delta\Delta E_{H^+}$ from the energy minimum for **3eH**, at $\tau \approx 0°$, may be compared with that derived for **4eH***cis* and **5eH***cis*. The hydrogen bond in **3eH** is replaced by unfavourable 4e$^-$ and dipole interactions due to the fluorine in **4eH***cis* and an unfavourable steric interaction plus a stabilizing hydrogen bond in **5eH***cis*. $\delta\Delta E_{H^+}$ increases from −2.39 to +1.66 to +2.70 kcal mol^{-1} for **3eH**, **5eH***cis* and **4eH***cis*, respectively (Table 3). This is compatible with the replacement of stabilizing by destabilizing interactions in these protonated equatorial conformers. These interactions are 'switched off' in equatorial conformers in which the imidazole ring is orthogonal to the C1′–O bond ($\tau_1 \approx \pm 90°$). Comparison of $\delta\Delta E_{H^+}$ for these conformers is extremely informative, since in the absence of the compound-specific interactions, underlying and general trends in the conformational equilibria of the imidazolides are revealed. Values of $\delta\Delta E_{H^+}$ for **3eH**⊥ and **4eH** are −1.13 and −1.14 kcal mol^{-1} respectively. There is thus an underlying shift in the equilibrium towards the equatorial conformer on protonation, even in the absence of specific hydrogen bonding stabilization of the protonated equatorial conformers, for both **3** and **4**. In each case, **3eH**⊥ and **4eH** (and also for **5eH**⊥), *N*-protonation is seen to result in a contraction of ∠O–C–N by 3.0°, 3.0° and 2.7°, respectively. Moreover, the ∠O–C–N bond angle is contracted by 6°–7° relative to the unprotonated axial conformers. Clearly, in this context, the value of $\delta\Delta E_{H^+}$ for **5eH**⊥, +0.60 kcal mol^{-1}, requires explanation. The value of $\delta\Delta E_{H^+}$ for **5eH**, +0.30 kcal mol^{-1}, also reflects a shift towards the axial conformer on protonation. In the 2-methyl system it is argued that special stabilization of **5aH** overwhelms the underlying stabilization of the protonated equatorial conformer. The proposed methyl H ··· O special stabilization of **5aH** is removed in the alternative conformer **5aH′**. The calculated $\delta\Delta E_{H^+}$ for **5aH′** and **5eH** (−0.88 kcal mol^{-1}) does indeed reveal the underlying stabilization of the equatorial conformer on *N*-protonation.

Computational Caveats.—Several caveats apply to the use of computational, molecular orbital methods focussed on experimental phenomena. The highest level of calculation employed in this study, MP2/6-31G*//HF/6-31G*, includes electron correlation and is comparable to methods employed in recent computational work on the anomeric effect. Data calculated at the HF/3-21G* level demonstrate similar trends to that calculated at the higher levels. The inclusion of the imidazole ring requires truncation of the pyranose moiety for calculations at the MP2 level. Some lack of accuracy might be predicted with the use of the truncated model compounds.

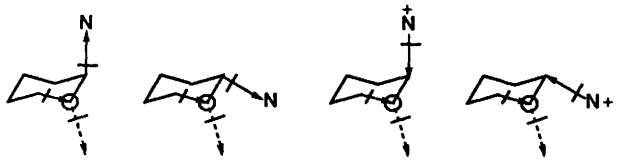

Scheme 3

However, the good agreement (*a*) with semiempirical calculations on the intact *N*-pyranosylimidazolides and (*b*) with experimental data, both support the use of the truncated models. In addition, the conclusions focus on trends in data or relative differences in conformational energy, rather than absolute energy differences between conformers. This is important in the light of the bias towards axial conformers, reported as a general feature of the 6-31G* basis set.[14] One possible flaw in the computational methodology is the exclusion of the counterion for the protonated imidazolides, which may influence electrostatic and solvation interactions.

Discussion

Several explanations of the reverse anomeric effect have been presented. Lemieux has stated that the original explanation was electrostatic; attributed to a through-space interaction of the positive charge associated with the anomeric substituent and the unshared electrons present on the ring oxygen.[27] Ironically, this is the explanation dictated by the results in the present work. Subsequently, a molecular orbital rationale has been offered.[28] Conversely, the dipole explanation of the reverse anomeric effect has been cited to support a similar dipole rationale of the Edward–Lemieux effect and the GAE, in place of the anomeric hyperconjugation, molecular orbital rationale.[6,12] The dipole explanation put forward by Lemieux and Morgan depicted interactions between the C3′–O and C1′–N1 bond dipoles, which would be unfavourable without *N*-protonation if these bonds were *gauche* (Scheme 3). An alternative common representation of the dipole rationale depicts an atomic dipole on oxygen caused by the directionality of the non-bonding electrons (Scheme 3). It has been pointed out that this is in effect an interaction between a monopole and the complementary end of a dipole. Thus the dipole and electrostatic explanations become equivalent. In this form both must be considered stereoelectronic effects, since the orientation of the n(O) electrons is the controlling factor. Recent computational work has stated support for the dipole argument[13] and the electrostatic explanation[15] of the reverse anomeric effect. However, all previous computational studies have focussed upon simple primary or secondary ammonium substituents at the anomeric carbon. Since *N*-protonation results in formation of a tetracoordinate centre directly bonded to the anomeric centre, the steric perturbation on protonation might be expected to be amplified in these species over their quaternary, heterocyclic ammonium counterparts in which the site of protonation is more distant. Indeed, Salzner and Schleyer argue that the equatorial preference of the $-NH_3^+$ substituent results largely from steric contributions.[14] The close spatial relationship of the vicinal hydrogen of the $-NH_2R^+$ substituent with the ring oxygen also allows a strong attractive interaction, as argued by Grein and Deslongchamps[15] and Kirby and Williams[29] among others. Imidazolide derivatives differ from the simple amines in that protonation occurs at the nitrogen distant from the anomeric centre. There is no large 1,3-diaxial, steric perturbation from addition of an atom geminal to the anomeric centre, nor the obvious, stabilizing, electrostatic interaction on addition of an acidic proton vicinal to the ring oxygen. Calculations on the imidazolides also allow direct comparison with the experimental data of Paulsen *et al.* on the reverse anomeric effect.[11]

Comparison of torsional profiles for the 2-fluoro- and unsubstituted imidazolides, **4aH**, **4eH**, **3a**, **3e**, **3aH**, demonstrates two strong contributions to conformational energy. The dominant contribution is a destabilizing steric effect, of greater magnitude in the axial conformers owing to the presence of 1,3-diaxial interactions with the imidazole substituent. Expansion of the O–C–N bond angle and to some extent lengthening of the C–N bond are correlated with minimization of steric interactions with the imidazole substituent. The second contribution is anomeric hyperconjugation, $n(O)\rightarrow\sigma^*(C–N)$ as confirmed by NBO analysis, which is again of much greater magnitude in the axial conformation, although also observed in the equatorial conformers. Changes in C–N and C–O bond length correlate with the magnitude of anomeric hyperconjugation on rotation about the C–O bond. Protonation influences both the steric and hyperconjugative effects. Lengthening of the C–N bond, due in part to the expected increase in anomeric hyperconjugation in the protonated imidazolides, reduces steric interactions with the imidazole substituent. Other contributions are present. A small $n(N)\rightarrow\sigma^*(C–O)$ interaction is indicated by NBO analysis in the unprotonated imidazolides. More importantly, the major contribution to the energy of the protonated equatorial imidazolide **3eH** is neither steric nor hyperconjugative, but electrostatic. The torsional energy profile of **3eH** correlates with the torsional dependence of the coulombic attraction between H2 and oxygen, with some evidence for interaction between C2 and oxygen. Moreover, removal of this H2 · · · O hydrogen bond on replacement of H2 with fluorine in **4eH**, causes the torsional profile to revert to that of the unprotonated equatorial imidazolides, **4e** and **3e**.

In the gas-phase calculations, anomeric hyperconjugation, despite the unfavourable steric contribution, dominates, resulting in an equilibrium favouring the axial conformer of the unprotonated imidazolide **3** at all levels of calculation. Increased anomeric hyperconjugation on protonation, reinforced by a smaller favourable change in the steric factor might be predicted to push the position of the equilibrium further towards the axial conformation on protonation. However, the opposite is observed. At the highest level of calculation employed, the equilibrium, on protonation, in fact shifts towards the equatorial conformer by 2.39 kcal mol^{-1} [$\delta\Delta E_{H^+}$ (**3**) = −2.39 kcal mol^{-1}]. It is the measure of the shift in the equilibrium (either $\delta\Delta E_{H^+}$ or ΔE_S) that is important (Tables 2, 3, Fig. 12). A negative value of $\delta\Delta E_{H^+}$ is indicative of a shift in equilibrium towards the equatorial conformer on protonation, which using the original definition of Lemieux, is equivalent to a reverse anomeric effect. Calculations employing solvation approximations demonstrate that solvation also has a profound impact on the position of this equilibrium; conformers with larger dipoles are stabilized by polar solvent. The shift in the equilibrium on changing to a more polar solvent favours the equatorial conformer (ΔE_S = −0.7 kcal mol^{-1}). But, the protonated axial conformer is more highly stabilized by a more polar solvent yielding a shift in equilibrium, instead, towards the axial conformer (ΔE_s = +1.3 kcal mol^{-1}). The predictions that result from these calculations are (*i*) increasing solvent polarity will lead to a shift in the equilibrium of the unprotonated imidazolide towards the equatorial conformer; (*ii*) protonation in a non-polar or low polarity solvent will lead to a shift in the equilibrium towards the equatorial conformer and (*iii*) in polar solvents, the shift in the equilibrium on protonation towards the equatorial conformer may be reversed.

Comparison with the experimental data of Paulsen *et al.* allows verification of (*i*) and (*ii*). For the glycosylimidazolides studies by NMR spectroscopy, the equilibrium shifts towards the equatorial conformer on increasing solvent polarity from

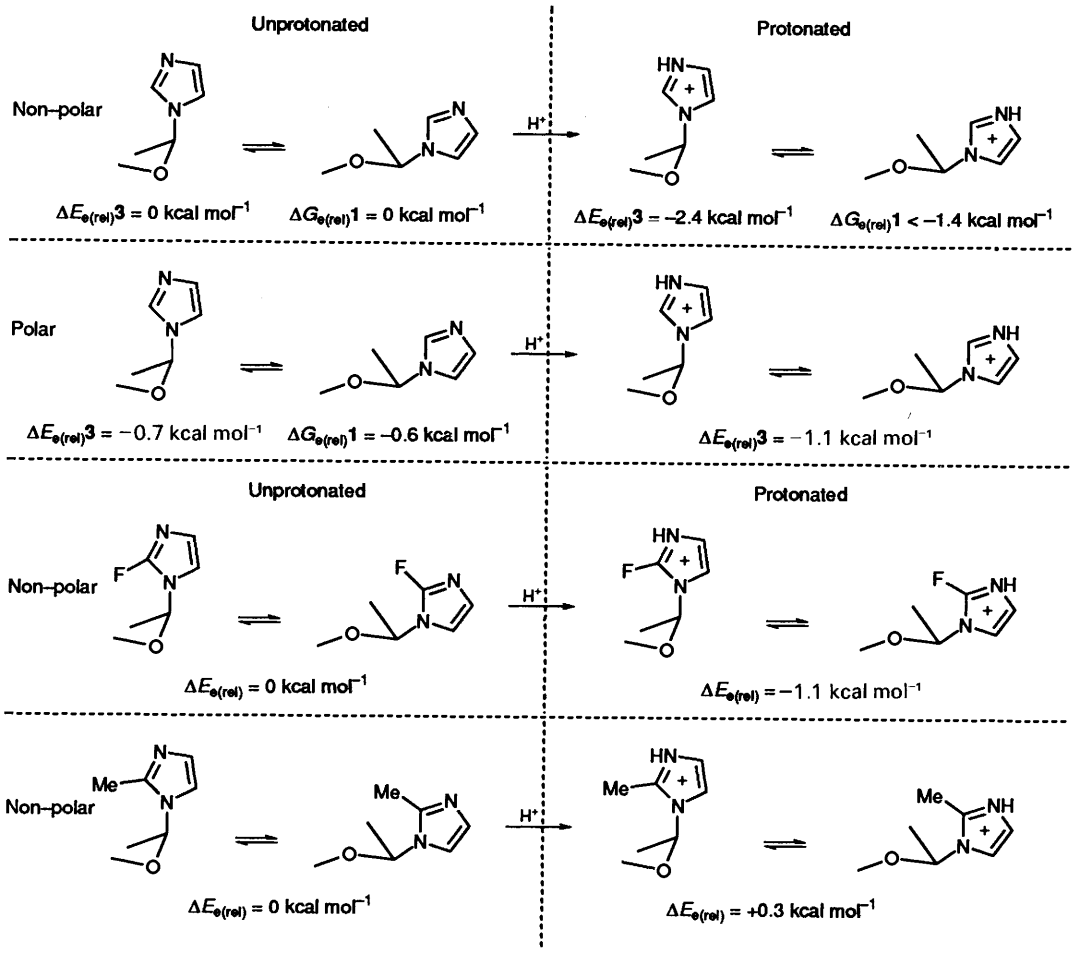

Fig. 12 Equilibrium shifts upon protonation and solvation for imidazolides **1**, **3**, **4**, **5**. ΔE_e(rel) is E(eq) − E(ax) and is set at zero for the equilibrium between the unprotonated isomers in the gas phase (or non-polar solvent). A negative value of ΔE_e(rel) indicates a shift in equilibrium towards the equatorial conformer; this corresponds to a reverse anomeric effect. All equilibria refer to minimum-energy conformers (Table 3). Values for **1** are calculated from the experimental data of Paulsen *et al.*[11] ΔG_e(rel) on protonation is a lower limit since the conformational ratio is given as >95%.

CCl_4 to $CDCl_3$ to $(CD_3)_2CO$. On protonation, by addition of trifluoroacetic acid to a $CDCl_3$ solution, the equilibrium shifts further towards the equatorial conformer, such that only the $^1C_4$ isomer is observed (>95%). The magnitude of the experimentally observed shifts in equilibrium is also in reasonable agreement with the calculated values (Fig. 12).

Clearly, both experiment and calculations are compatible with the presence of a reverse anomeric effect in *N*-pyranosylimidazolides for which **2** and **3** are models. It remains to attribute a rationale to this effect. The protonated equatorial imidazolide **3eH** is strongly influenced by a favourable electrostatic contribution, which is not a dominant factor in any of the other structures **3a**, **3e**, **3aH**. If the H2 · · · O hydrogen bond is the cause of the observed reverse anomeric effect, removal of this stabilizing interaction would result in the disappearance of any reverse anomeric effect. Such an observation would require the discarding or at least redefining of the term reverse anomeric effect. Both rotation of the imidazolium ring in **3eH**⊥ to a position orthogonal to oxygen, and substitution of H2 in the 2-fluoroimidazolide, **4**, serve to eliminate the H2 · · · O hydrogen bond. Nevertheless, although of diminished size, we still observe the persistence of the reverse anomeric effect in each of these systems, including the 2-substituted imidazolide. Protonation leads to a shift in the equilibrium towards the equatorial conformer by 1.13 and 1.14 kcal mol^{-1} for **3eH**⊥ and **4**, respectively. It seems reasonable that the H2 · · · O bond contributes towards the reverse anomeric effect in **3**, but that the effect is more general and does not require this specific hydrogen-bond. Examination of stabilizing molecular orbital interactions in the NBO analysis reveals no strong charge transfer interactions that might account for a relative stabilization of the protonated equatorial conformer. Although dipole interactions may influence molecular energy, we, as other workers, have detected no clear correlation between energy and molecular dipole moment.[14] The proximity of the electron density, associated with the non-bonding electrons on oxygen, and the face of the imidazole ring in the equatorial conformation is shown by examination of simple molecular models and more vividly by electrostatic potential maps (Fig. 11). In the axial conformation, this centre of electron density is held away from the face of the heterocyclic ring. NBO analysis reveals no significant charge-transfer interactions involving n(O) donor and ring acceptor orbitals. Thus it is argued that the simple electrostatic interaction between the positively charged imidazolium ring and the electron density on oxygen is maximized in the equatorial conformation. This conclusion is supported by changes in bond angles on protonation.

If we consider $\delta\Delta E_{H^+}$(**5aH'**) the shift in equilibrium of 0.88 kcal mol^{-1} towards the equatorial isomer on *N*-protonation again indicates the presence of a reverse anomeric effect. However, the small electrostatic stabilization that causes the reverse anomeric effect is counterbalanced in the 2-methyl imidazolides by electrostatic stabilization of the axial minimum energy conformer, **5aH**, on *N*-protonation. The calculated value of $\delta\Delta E_{H^+}$(**5aH**) is positive, indicating the absence of a reverse

anomeric effect in 2-methylimidazolides, even in the gas phase and non-polar solvent. The conformational equilibria of the simple model systems studied are highly sensitive to intramolecular electrostatic effects, which are dictated by intramolecular steric effects. The addition of substituents to the pyranose ring may therefore significantly influence conformational equilibria.

Conclusions

The axial conformation in the *N*-pyranosylimidazolide models is dominated by anomeric hyperconjugation and 1,3-diaxial steric contributions. The 1,3-diaxial interaction opposes the adoption of conformations that permit hydrogen-bonding between oxygen and either H2 or H5 of the imidazole ring. The *gauche* arrangement of C3′–O and C1′–N1 bonds in the axial conformation minimizes favourable electrostatic interactions between electron density associated with non-bonding electrons on oxygen and the positively charged imidazolium ring. The influence of both anomeric hyperconjugation and steric interactions is greatly reduced in the equatorial conformation. Thus specific hydrogen-bonding of ring hydrogens to oxygen is possible with little steric cost. The *trans* arrangement of C3′–O and C1′–N1 bonds in the equatorial conformation maximizes favourable electrostatic interactions between electron density associated with non-bonding electrons on oxygen and the positive imidazolium ring. *N*-Protonation places significant positive charge across the imidazole ring and ring hydrogens leading to dominant electrostatic stabilization in the equatorial conformer and a shift in equilibrium towards the equatorial conformation. This equilibrium shift is compatible with the phenomenon of the reverse anomeric effect. The magnitude of these electrostatic effects is small and the presence of stabilizing electrostatic effects in axial conformers on *N*-protonation may reverse the shift in equilibrium and negate the reverse anomeric effect. The rationale thus provided predicts that observation of the reverse anomeric effect will not be universal for heterocyclic anomeric substituents bearing a positive charge, even in the gas phase, but that electrostatic stabilization of the equatorial conformer on protonation will be a universal contribution to conformational energy. Calculations including solvation predict that the shifts in conformational equilibria are highly solvent dependent: any reverse anomeric effect is likely to disappear as solvent polarity is increased.

Supplementary Material Available.—Cartesian coordinates for all minimum-energy structures in Table 1 and energies and structural data for all rotamers of **3** for which figures are presented have been deposited with the British Library (Supp. No. 57058; 9 pages). For details of the Supplementary Publications Scheme see 'Instructions for Authors (1995)', *J. Chem. Soc., Perkin Trans. 2*, 1995, issue 1.

Note Added in Proof.—An experimental NMR analysis of anomers of *N*-glucosylimidazolides has recently been communicated (M. A. Fabian, C. L. Perrin, M. L. Sinnott, *J. Am. Chem. Soc.*, 1994, **116**, 8398). The anomerization equilibria described are compatible with the data from the present computational work.

Acknowledgements

Queen's University and the Natural Sciences & Engineering Research Council of Canada are thanked for financial support. Professor Mario Pinto is thanked for discussion of his work prior to publication. Professor Carmay Lim is thanked for providing a copy of the CDM program code.

References

1 G. R. J. Thatcher, *The Anomeric Effect and Associated Stereoelectronic Effects*, ed. G. R. J. Thatcher, ACS Symposium Series No. 539, ACS, Washington DC, 1993; E. Juaristi, G. Cuevas, *Tetrahedron* 1992, **48**, 5019; P. Deslongchamps, *Stereoelectronic Effects in Organic Chemistry*, Pergamon, Oxford, 1983; A. J. Kirby, *The Anomeric Effect and Related Stereoelectronic Effects at Oxygen*, Springer, Verlag, Berlin, 1983.
2 J. T. Edward, *Chem. Ind. (London)*, 1955, 1107; R. U. Lemieux and N. J. Chu, *Abstr. Pap. Am. Chem. Soc. Meeting*, 1958, **33**, 31N; J. T. Edward, *The Anomeric Effect and Associated Stereoelectronic Effects*, ed. G. R. J. Thatcher, ACS Symposium Series No. 539, 1–5, ACS, Washington DC, 1993.
3 R. U. Lemieux, A. A. Pavia, J. C. Martin and K. A. Watanabe, *Can. J. Chem.*, 1969, **47**, 4427; R. U. Lemieux, *Anomeric Effect: Origin and Consequences*, eds. W. A. Szarek and D. Horton, ACS Symposium Series No. 87, Ch. 2, ACS, Washington DC, 1979.
4 R. U. Lemieux, *Pure Appl. Chem.*, 1971, **25**, 527; R. U. Lemieux and A. R. Morgan, *Can. J. Chem.*, 1965, **43**, 2205.
5 R. Jalluri, Y. H. Yuh and E. W. Taylor, *The Anomeric Effect and Associated Stereoelectronic Effects*, ed. G. R. J. Thatcher, ACS Symposium Series No. 539, 277–293, ACS, Washington DC, 1993.
6 (*a*) C. L. Perrin, *The Anomeric Effect and Associated Stereoelectronic Effects*, ed. G. R. J. Thatcher, ACS Symposium Series No. 539, 70–96, ACS, Washington DC, 1993; (*b*) C. L. Perrin and K. B. Armstrong, *J. Am. Chem. Soc.*, 1993, **115**, 6825.
7 J.-P. Praly and R. U. Lemieux, *Can. J. Chem.*, 1987, **65**, 213; R. W. Franck, *Tetrahedron*, 1983, **39**, 3251; E. Juaristi, N. A. Lopez-Nunez, R. S. Glass, A. Petsom, R. O. Hutchins and J. P. Stercho, *J. Org. Chem.*, 1986, **51**, 1357.
8 For references see, G. R. J. Thatcher, *The Anomeric Effect and Associated Stereoelectronic Effects*, ed. G. R. J. Thatcher, ACS Symposium Series No. 539, 6–25, ACS, Washington DC, 1993.
9 B. M. Pinto and R. Y. N. Leung, *The Anomeric Effect and Associated Stereoelectronic Effects*, ed. G. R. J. Thatcher, ACS Symposium Series No. 539, 126–155, ACS, Washington DC, 1993.
10 M. C. Krol, J. M. C. Huige and C. Altona, *J. Comput. Chem.*, 1990, **11**, 765.
11 H. Paulsen, Z. Gyorgdeak and M. Friedmann, *Chem. Ber.*, 1974, **107**, 1590.
12 M. L. Sinnott, *Adv. Phys. Org. Chem.*, 1988, **24**, 113.
13 C. J. Cramer, *J. Org. Chem.*, 1992, **57**, 7034.
14 U. Salzner, P. v. R. Schleyer, *J. Org. Chem.*, 1994, **59**, 2138.
15 F. Grein and P. Deslongchamps, *Can. J. Chem.*, 1992, **70**, 1562; F. Grein, *The Anomeric Effect and Associated Stereoelectronic Effects*, ed. G. R. J. Thatcher, ACS Symposium Series No. 539, 205–226, ACS, Washington DC, 1993.
16 J. P. Foster and F. Weinhold, *J. Am. Chem. Soc.*, 1980, **102**, 7211; A. E. Reed and F. Weinhold, *J. Chem. Phys.*, 1983, **78**, 4066; A. E. Reed, R. B. Weinstock and F. Weinhold, *J. Chem. Phys.*, 1985, **83**, 735; J. E. Carpenter and F. Weinhold, *J. Mol. Struct. (Theochem.)*, 1988, **169**, 41.
17 For example, A. E. Reed and P. v. R. Schleyer, *Inorg. Chem.*, 1988, **27**, 3969; see also P. A. Petillo and L. E. Lerner, *The Anomeric Effect and Associated Stereoelectronic Effects*, ed. G. R. J. Thatcher, ACS Symposium Series No. 539, 156–175, ACS, Washington DC, 1993.
18 M. J. S. Dewar, E. G. Zoebisch, E. F. Healy and J. J. P. Stewart, *J. Am. Chem. Soc.*, 1985, **107**, 3902.
19 SPARTAN v.3.0, Wavefunction, Inc. 18401 Von Karman, #210, Irvine, CA, 92715.
20 GAUSSIAN 92, Revision C., M. J. Frisch, G. W. Trucks, M. Head-Gordon, P. M. W. Gill, M. W. Wong, J. B. Foresman, B. G. Johnson, H. B. Schlegel, M. A. Robb, E. S. Replogle, R. Gomperts, J. L. Andes, K. Raghavachari, J. S. Binkley, C. Gonzalez, R. L. Martin, D. J. Fox, D. J. DeFrees, J. Baker, J. J. P. Stewart and J. A. Pople, Gaussian, Inc., Pittsburgh, PA, 1992.
21 W. J. Pietro, M. M. Francl, W. J. Hehre, D. J. DeFrees, J. A. Pople and J. S. Binkley, *J. Am. Chem. Soc.*, 1982, **104**, 5039; P. C. Hariharan and J. A. Pople, *Chem. Phys. Lett.*, 1972, **66**, 217.
22 J. S. Binkley and J. A. Pople, *Int. J. Quantum. Chem.*, 1975, **9**, 229.
23 C. M. Breneman and K. B. Wiberg, *J. Comput. Chem.*, 1990, **11**, 361.
24 C. J. Cramer and D. G. Truhlar, *Science*, 1992, **256**, 213; R. W. Dixon, J. M. Leonard and W. J. Hehre, *Isr. J. Chem.*, 1994, **33**, 692.
25 S. L. Chan and C. Lim, Dept. of Molecular & Medical Genetics,

University of Toronto, King's College Circle, Toronto M5S 1A8, Canada; see S. L. Chan, C. Lim, *J. Phys. Chem.*, 1994, **98**, 692.
26 K. B. Wiberg and M. Marquez, *J. Am. Chem. Soc.*, 1994, **116**, 2197; W. L. Jorgensen, P. I. Morales de Tirado and D. L. Severance, *J. Am. Chem. Soc.*, 1994, **116**, 2199; S. Ha, J. Gao, B. Tidor, J. W. Brady and M. Karplus, *J. Am. Chem. Soc.*, 1991, **113**, 1553.
27 R. U. Lemieux, *Explorations with Sugars: How Sweet It Was, Profiles, Pathways and Dreams*, ed. J. I. Seeman, ACS, Washington DC, 1990.
28 S. David, O. Eisenstein, W. J. Hehre, L. Salem and R. Hoffman, *J. Am. Chem. Soc.*, 1973, **95**, 3806.
29 A. J. Kirby and N. H. Williams, *The Anomeric Effect and Associated Stereoelectronic Effects*, ed. G. R. J. Thatcher, ACS Symposium Series No. 539, 55–69, ACS, Washington DC, 1993.

Paper 4/04826A
Received 5*th August* 1994
Accepted 20*th October* 1994